This article was downloaded by: *10.2.97.136*
On: 08 Dec 2023
Access details: *subscription number*
Publisher: *CRC Press*
Informa Ltd Registered in England and Wales Registered Number: 1072954 Registered office: 5 Howick Place, London SW1P 1WG, UK

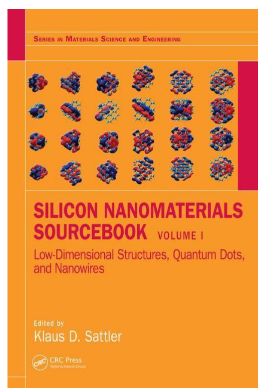

Silicon Nanomaterials Sourcebook
Low-Dimensional Structures Nanopowders, Nanowires
Klaus D. Sattler

Nanocrystalline silicon thin films

Publication details
https://test.routledgehandbooks.com/doi/10.4324/9781315153544-5
Atif Mossad Ali, Takao Inokuma
Published online on: 09 Aug 2017

How to cite :- Atif Mossad Ali, Takao Inokuma. 09 Aug 2017, *Nanocrystalline silicon thin films from:* Silicon Nanomaterials Sourcebook, Low-Dimensional Structures Nanopowders, Nanowires CRC Press
Accessed on: 08 Dec 2023
https://test.routledgehandbooks.com/doi/10.4324/9781315153544-5

PLEASE SCROLL DOWN FOR DOCUMENT

Full terms and conditions of use: https://test.routledgehandbooks.com/legal-notices/terms

This Document PDF may be used for research, teaching and private study purposes. Any substantial or systematic reproductions, re-distribution, re-selling, loan or sub-licensing, systematic supply or distribution in any form to anyone is expressly forbidden.

The publisher does not give any warranty express or implied or make any representation that the contents will be complete or accurate or up to date. The publisher shall not be liable for an loss, actions, claims, proceedings, demand or costs or damages whatsoever or howsoever caused arising directly or indirectly in connection with or arising out of the use of this material.

4 Nanocrystalline silicon thin films

Atif Mossad Ali and Takao Inokuma

Contents

4.1 Introduction 97
4.2 Experiment 97
4.3 Crystalline Properties Depending on Deposition Conditions Found in Previous Works 98
4.4 Results and Discussion 100
4.4.1 Structural Characterization 100
4.4.2 Additional Discussion of the Growth Mechanisms of nc-Si 104
4.5 Conclusion 105
References 105

4.1 INTRODUCTION

Silicon is at the heart of the microelectronics. Its dominance over other semiconductors is intimately tied to its superior materials and process, and to the tremendous base of technology that has developed around it. A recent trend toward development of nanocrystalline silicon (nc-Si) lies in preparing nc-Si thin films exhibiting strong photoluminescence, based on a quantum size effect (Ali et al. 2002). This technique is expected to have a potential for application to optoelectronics. In addition, as crystallites are decreased in size to the nanoscale level, their electronic and vibrational properties will be modified, then the surface and quantum size effects play an important role. Formation of nc-Si structures has been tried utilizing various techniques: anodic oxidation of crystalline Si, that is, formation of porous Si formation of nc-Si thin films using plasma-enhanced chemical vapor deposition (PECVD), sputtering, evaporation, and ion beam synthesis. Furthermore, nc-Si thin films can be obtained by the thermal crystallization of amorphous Si films or Si-rich oxide films.

Study of the effects of the different and various deposition parameters on the growth of the material, and also the growth mechanisms, are therefore important both for newer device applications and also for understanding the basic physics of the growth process of Si thin films (Ali et al. 2002). Several deposition parameters, such as substrate temperature, gas flow rate, radio frequency (rf) power, dilution of the source gas (silane) with other gases (argon, hydrogen, or helium), plasma energy and density, and deposition pressure will strongly influence the structure and properties of the grown nc-Si thin films.

In the case of PECVD nc-Si thin films deposited using $SiH_4/SiF_4/H_2$ gas mixtures, the etching effects of H- and F-radicals in plasma will play important roles. Such etching effects may result in different mechanisms that affect crystallinity. However, the growth mechanisms of the nc-Si thin films are still unclear. In this chapter, we focus on the mechanisms of crystallization, through the understanding of the roles of H and F atoms in plasma under different plasma conditions.

4.2 EXPERIMENT

Nc-Si thin films were deposited using a $SiH_4/SiF_4/H_2$ gas mixture by PECVD. The substrates were cleaned for 40 min using nitrogen plasma and hydrogen plasma, respectively, just before deposition of films. The samples

Downloaded By: 10.2.97.136 At: 19:24 08 Dec 2023; For: 9781315153544, chapter4, 10.4324/9781315153544-4

were deposited on corning glass substrates for measurements of X-ray diffraction (XRD) and Raman scattering, and on n-type (100) Si substrates for measurements of Fourier transform infrared (FT-IR) absorption. The deposition temperature (T_d) values were varied from ~100 to 500°C. Furthermore, we adopted two different series for H_2 values: for series A, a large H_2 condition was selected, as SiF_4 = 0.38 sccm and H_2 = 30 sccm, and we also selected a condition without H_2 addition for series B, as SiF_4 = 0.5 sccm.

The structural properties were investigated using an XRD instrument (SHIMADZU XD-D1). The average grain size, $<\delta>$, was estimated using Scherrer's formula (Cullity 1978) from the width of the XRD spectra.

$$<\delta> = \frac{0.9\lambda}{B\cos\Theta_B}, \tag{4.1}$$

where λ is wavelength of the X-ray (1.54 Å), B the half-value width of the XRD spectral peak, and Θ_B the Bragg angle.

The Raman spectra were measured by a Raman spectrometer having a double monochrometer (Jobin Yvon RAMANOR HG 2S) coupled with a cooled photomultiplier tube (Hamamatsu R649S) and excited with an Ar-ion laser light at 488 nm. The crystallinity of the films, ρ, was estimated from the intensity of Raman spectra by the procedure proposed by Tsu et al. (1982) that is, a Raman spectrum was decomposed into two components of crystalline Si (c-Si) phase occurring at around 520 cm^{-1} and the amorphous Si (a-Si) phase at around 480 cm^{-1}, and then the ρ values were estimated from the intensity ratio of the above two components using the ratio of the integrated Raman cross section for crystalline and amorphous phases as follows:

$$\rho = \frac{I_c}{(I_c + I_a)} \tag{4.2}$$

where I_c is the Raman integrated intensity for the crystalline component (sharp peak at 520 cm^{-1}), and I_a is for amorphous phase (smooth peak at 480 cm^{-1}).

The vibrational spectra were measured by an FT-IR spectrometer (JASCO FT/IR-610). The density of given bonds can be estimated by the following method (Milovzorov et al. 1998):

$$N_{SiM} = \sum_{\nu} A_{\Omega}^{\nu} I_{\Omega}^{\nu} (M = \text{H or O}) \tag{4.3}$$

where A_{Ω}^{ν} is proportionality coefficient and I_{Ω}^{ν} is the intensity of the absorption IR spectrum from SiM bonds with the frequency ν, Ω configuration of Si atom's bonds.

4.3 CRYSTALLINE PROPERTIES DEPENDING ON DEPOSITION CONDITIONS FOUND IN PREVIOUS WORKS

As mechanisms causing influence on the crystalline properties, the following might be proposed: (1) an effect of chemical etching on the growing surface of the films (Okada et al. 1989; Tsai et al. 1989; Hasegawa et al. 1990; Kim et al. 1995; Ali et al. 2002), (2) an effect of chemical cleaning for removing impurities (Meyerson et al. 1990; Nagahara et al. 1992; Syed et al. 1997), (3) an effect of different surface morphology of the substrate (Arai et al. 1996; Hu et al. 1996; Kondo et al. 1996; Syed et al. 1997; Hasegawa et al. 1998a; Syed et al. 1999), and (4) an effect of hydrogen coverage, being related to the surface migration of adsorbates (Matsuda 1983; Nagamine et al. 1987; Kim et al. 1995). However, it has been suggested that the etching effects (mechanism 1) are more important in forming a crystalline structure rather than the effect of the hydrogen coverage (mechanism 4) (Okada et al. 1989; Tsai et al. 1989; Baert et al. 1992). Then hydrogen and fluorine, included in the feed gases used in the present work, are known to act as etchants for Si. So, in the abovementioned mechanisms, mechanism

Downloaded By: 10.2.97.136 At: 19:24 08 Dec 2023; For: 9781315153544, chapter4, 10.4324/9781315153544-5

(1) should accompany a change in the deposition rate. Indeed, the increase in the H_2 or SiF_4 flow rate, H_2 (Kim et al. 1995) or SiF_4 (Ali et al. 1999), decreased the deposition rates. Furthermore, as mechanism (1) acts to roughen the substrate surface at the initial stage of the film growth, mechanism (1) should then be closely related to mechanism (3). This roughened surface would also increase the nucleation rate, and the roughness depends on the range of T_d used. By contrast, the smooth surface of substrates would result in an increase in δ (Syed et al. 1997). This is because the etching efficiency due to H- and F-related radicals for Si films depends on T_d (Kim et al. 1991; Lim et al. 1996), as mentioned at a later stage.

On the other hand, crystalline Si films can be prepared by repeating, in cycles, film deposition and H-plasma (Srinivasan and Parsons 1998) or He-plasma exposure (Lee et al. 1996). Based on the former results, it has been suggested that the removal of hydrogen from the growing surface of films is essential for the improvement in the crystalline properties (Srinivasan and Parsons 1998). Based on the latter results, the crystallization of the surface layer in films after He-plasma exposure was important to the crystalline properties of the resultant Si films (Lee et al. 1996). These results also support the above mentioned model that effects of the etching along with those of ion-bombardment, due to H- or F-radicals, are more important. In addition, it has been reported that the etch rate by H-radicals decreases with increasing T_d (Kim et al. 1991), but the etch rate by F-radicals increases with T_d (Lim et al. 1996). Therefore, the addition of H- or F-related molecules to the feed gases under different T_d conditions would play an important role in the crystallization of Si films (Ali et al. 2002).

The H_2 addition under $T_d \geq 300$°C resulted in smaller δ and greater ρ values with increasing H_2 values (Kim et al. 1995; Milovzorov et al. 1998). In addition, both the (111)- and (110)-textured δ values were found to decrease with H_2 (Milovzorov et al. 1998). By contrast, under $T_d < 300$°C, only the (111) texture was observed (Hasegawa et al. 1998b; Milovzorov et al. 1998; Ali et al. 1999; Ali et al. 2001). However, both δ and ρ values have the respective maximum values at a given H_2 value (Milovzorov et al. 1998), or increase with increasing H_2 (Ali et al. 2001). For these films, the following conditions were used: H_2 = 50–300 sccm, SiF_4 = 3 sccm, SiH_4 = 0.09 sccm, and T_d = 330°C (Kim et al. 1995), H_2 = 10–46 sccm, SiF_4 = 0.13 sccm, SiH_4 = 0.6 sccm, and T_d = 100 and 300°C (Milovzorov et al. 1998), and H_2 = 5–30 sccm, SiF_4 = 0.1 sccm, SiH_4 = 0.5 sccm, and T_d = 100 and 220°C (Ali et al. 2001). Thus, rather small fixed SiF_4 values, compared with the range of H_2 used, were applied for these films so that the effect of F atoms may be eliminated, due to the formation of more stable HF bonds in the gas phase. The increase in δ and ρ with H_2 became slow as T_d increased from 100 to 220°C (Ali et al. 2001). Therefore, it is suggested that both δ and ρ values are likely to increase with increasing H_2 under lower T_d conditions. However, as a result of the present work, the increase in H_2 under low T_d was found to cause only the increase in the XRD intensities or ρ. Furthermore, the crystalline properties should also be affected by F-radicals as etchants as well as the effect of H_2 addition, causing mechanism (1) or (3).

The δ and ρ values as a function of SiF_4 exhibited different behaviors, depending on SiH_4 and/or T_d (Syed et al. 1997; Ali et al. 1999). For conditions of T_d = 400°C and H_2 = 0 sccm, Syed et al. (1997) found that both the δ and ρ values for films with SiH_4 = 1 sccm increased as SiF_4 increased from 0 to 0.5 sccm, while those for SiH_4 = 0.15 sccm monotonically decreased with SiF_4 (Syed et al. 1997). Furthermore, they found that the (110)-textured grains for SiH_4 = 1 sccm were preferentially grown as SiF_4 increased, while that for SiH_4 = 0.15 sccm weakened. Based on these results, they proposed that the changes in δ and ρ values were controlled by a change in the surface morphology of substrates, due to F-radicals (mechanism 3). Furthermore, in a previous work (Hasegawa et al. 1998a), in which the surface of substrates were pretreated by exposing them in H_2, N_2, and/or CF_4-He plasma, all Si films were deposited under the same conditions. As a result, the increases in δ and ρ were found as the Si films were deposited on substrates with a proper degree of surface roughness. In addition, it has also been reported that an excess supply of F-radicals will in turn deteriorate the crystalline properties (Kakinuma et al. 1995). On the other hand, when T_d decreased to 100°C under the conditions of SiH_4 = 0.6 sccm and H_2 = 40 sccm, the δ and ρ values as a function of SiF_4 (= 0 – 0.5 sccm) had the respective minimum values at SiF_4 = 0.1 sccm (Ali et al. 1999). The changes in δ and ρ were interpreted in terms of a difference in the etch rate due to H- and F-radicals (Ali et al. 1999), depending on T_d (Kim et al. 1991; Lim et al. 1996), which is related to mechanism (1) or (3).

Downloaded By: 10.2.97.136 At: 19:24 08 Dec 2023; For: 9781315153544, chapter4, 10.4324/9781315153544-5

On the other hand, Toyoshima et al. (1989) examined the changes in the crystallization behavior of microwave PECVD Si films by varying SiH_4 (= 5–50 sccm) and T_d (= 100–300°C) under fixed H_2 (= 450 sccm). They found that formation of (110) or (111) grains, respectively, will be enhanced as T_d increases or SiH_4 decreases, in which they proposed that the decrease in SiH_4 is tantamount to the excess supply of H-radicals. Furthermore, under the conditions without SiF_4 addition (SiH_4 = 1 sccm, SiF_4 = 0, H_2 = 3 sccm, and T_d = 150–750°C) (Hasegawa et al. 1998b), it has been shown that the dominant texture changed from the (111) orientation under low T_d conditions below 550°C and to the (110) orientation under high T_d above 550°C, in agreement with the results found in a previous work (Toyoshima et al. 1989). In addition, the addition of H- and F-related molecules to the feed gases has been reported to lower T_d for obtaining crystalline Si films (Kakinuma et al. 1995; Lim et al. 1996; Hasegawa et al. 1998a; Milovzorov et al. 1998). Furthermore, the crystalline properties of PECVD Si films appear to vary as a direct function of T_d. In previous articles, both δ and ρ values have been shown to increase as T_d increases from 100 to 300°C under SiH_4 = 0.6 sccm, SiF_4 = 0.13 sccm, and H_2 = 10 to 46 sccm (Milovzorov et al. 1998), and from 250 to 400°C under SiH_4 = 10 sccm, SiF_4 = 400 sccm, and H_2 = 500 sccm (Kakinuma et al. 1995). By contrast, Lim et al. (1996) have found a decrease in δ and a fixed ρ value as T_d increases from 280 to 450°C under SiH_4 = 0.1 sccm, SiF_4 = 3.5 sccm, and H_2 = 1 sccm. Furthermore, Syed et al. (1999) have found rather complex behaviors of δ and ρ values as a function of T_d (= 150–400°C) under SiH_4 = 1 sccm, SiF_4 = 0.5 sccm, and H_2 = 0 or 5 sccm, that is, both the (110) δ and the ρ values for H_2 = 5 sccm had the maximum values at around T_d = 300°C and monotonically increased with T_d for H_2 = 0 sccm. As a consequence, the (110)-textured δ value appears to be enhanced with an increase in T_d (Toyoshima et al. 1989; Kakinuma et al. 1995; Hasegawa et al. 1998a; Syed et al. 1999) or SiF_4 (Syed et al. 1997), or a decrease in H_2 (Milovzorov et al. 1998), or an increase in SiH_4 (Toyoshima et al. 1989). In addition, the (110)-XRD intensities have also been reported to increase with increasing T_d (Hasegawa et al. 1998b; Syed et al. 1999), or SiF_4 (Syed et al. 1997). Thus, the change in the texture (or occurrence of different textures in crystal grains) of the films may be closely related to the change in the crystallization process. So, the changes in the crystalline properties such as δ, ρ, and the texture, depending on the deposition conditions, are rather complex, but the mechanisms are not clear.

4.4 RESULTS AND DISCUSSION

4.4.1 STRUCTURAL CHARACTERIZATION

Figure 4.1 shows the average grain size, (a) $\langle\delta(111)\rangle$ and (b) $\langle\delta(110)\rangle$, obtained from the (111) and (110) XRD spectra, respectively, as a function of T_d, for series A films (closed triangles) and series B films (closed circles) (Ali et al. 2002). As shown in Figure 4.1, both the $\langle\delta(111)\rangle$ and the $\langle\delta(110)\rangle$ values for series A films and the $\langle\delta(110)\rangle$ values for series B films monotonically increase with increasing T_d, while the $\langle\delta(111)\rangle$ values for series B films have a maximum value at around T_d = 200–250°C. Figure 4.2 shows (a) the (111) and (b) the (110) XRD intensities, as a function of T_d, for series A films (closed triangles) and series B films (closed circles) shown in Figure 4.1. As shown in Figure 4.2a, the (111) XRD intensities for series A films monotonically decrease with increasing T_d, while those for series B films appear to have a minimum value at around T_d = 200–250°C, in good correspondence to the change in $\langle\delta(111)\rangle$ (Figure 4.1a). By contrast, the (110) XRD intensities for series A films show the increase with T_d up to 300°C, followed by the saturation, but those for series B films monotonically increase with T_d. Furthermore, it is found that both the (111) and (110) XRD intensities for series A films are larger than those for series B films, especially under low T_d conditions as seen in Figure 4.2, that is, the volume of both textured crystalline phases in the films is expected to be enhanced as H_2 increases.

Figure 4.3 shows (a) the peak frequency, E_R, of the Raman signal arising from the c-Si phase and (b) ρ, as a function of T_d, for series A films (closed triangles) and series B films (closed circles) shown in Figure 4.1 (Ali et al. 2002). As shown in Figure 4.3a, the values of E_R for series A and B films increase with an increase in T_d up to T_d = 150°C. After the saturation of E_R at around E_R = 519 cm^{-1} for both series films, the E_R values for series A films increase with T_d up to E_R = 522 cm^{-1} at T_d = 300°C and then slightly decrease again.

Downloaded By: 10.2.97.136 At: 19:24 08 Dec 2023; For: 9781315153544, chapter4, 10.4324/9781315153544-5

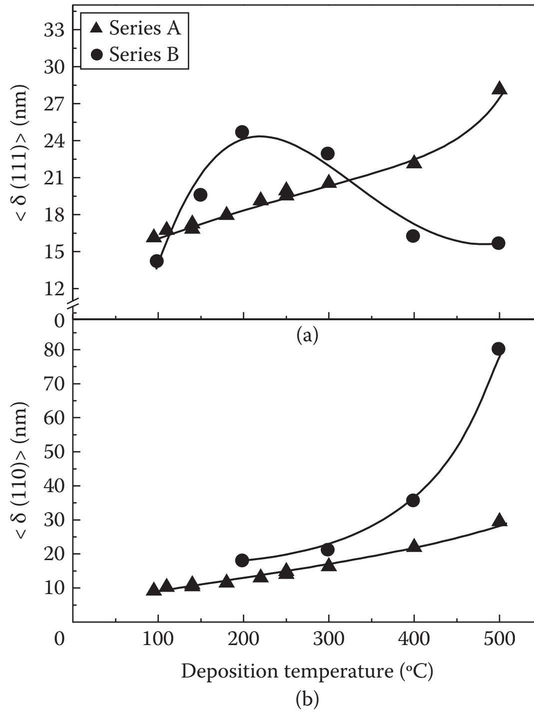

Figure 4.1 (a) Average grain size, <δ(111)> and (b) <δ(110)>, obtained from the <111> and <110> XRD spectra, respectively, as a function of *T*d, for series A films (closed triangles) and series B films (closed circles). (From Ali, A.M., et al., *Jpn. J. Appl. Phys*., 41, 169–175, 2002.)

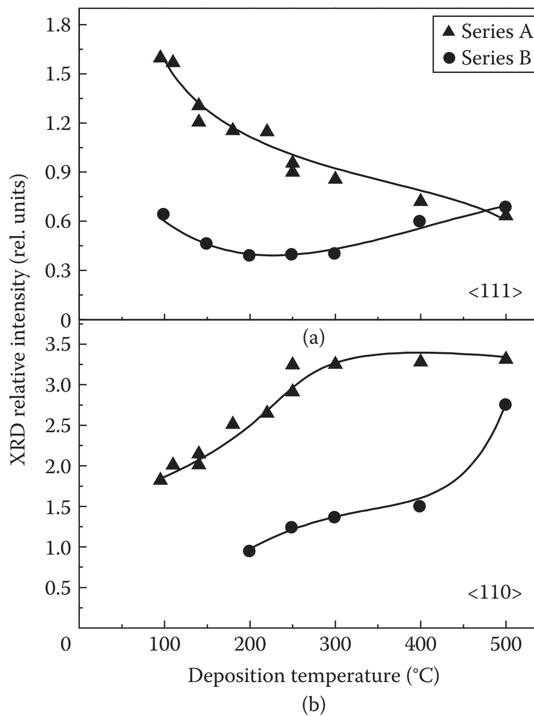

Figure 4.2 Integrated intensities for the <111> and <110> XRD spectra, respectively, (a) <111> XRD intensities and (b) <110> XRD intensities, as a function of *T*d, for series A films (closed triangles) and series B films (closed circles).

Downloaded By: 10.2.97.136 At: 19:24 08 Dec 2023; For: 9781315153544, chapter4, 10.4324/9781315153544-5

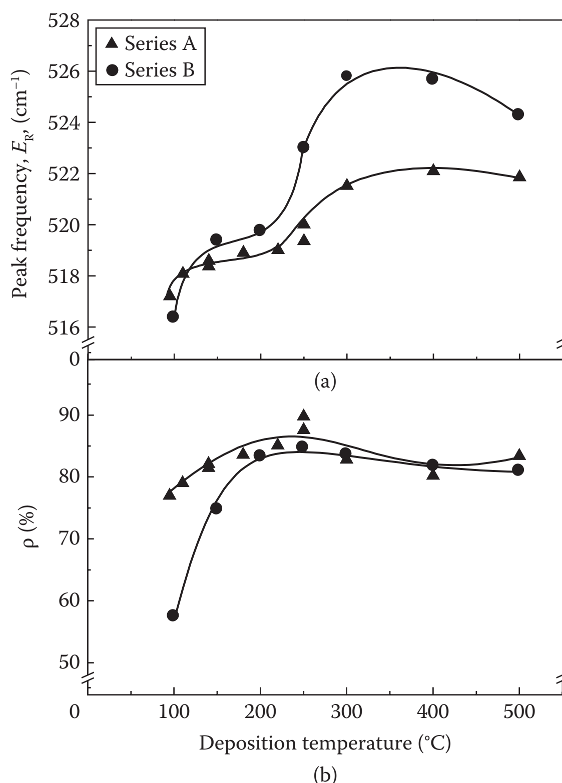

Figure 4.3 (a) Peak frequency, *ER*, of the Raman signal arising from the crystalline Si phases and (b) crystalline volume fraction, r, as a function of *Td*, for series A films (closed triangles) and series B films (closed circles). (From Ali, A.M., et al., *Jpn. J. Appl. Phys.*, 41, 169–175, 2002.)

On the other hand, the E_R values for series B films increase with T_d up to E_R = 526 cm^{-1} at T_d = 300°C and then decrease. As shown in Figure 4.3b, the ρ values for both series A and B films increase as T_d increases in T_d < 250°C and then slightly decrease again, in correspondence with the change in the XRD intensities (Figure 4.2). However, a relationship between the changes in XRD intensities and that in ρ for T_d > 250°C are rather complex. Figure 4.4 shows the full width at half maximum (FWHM) of the 520 cm^{-1} component in a Raman signal, as a function of T_d, for series A films (closed triangles) and series B films (closed circles) shown in Figure 4.1. As seen in Figure 4.4, the FWHM values for both series films monotonically decrease with increasing T_d.

Figure 4.5 illustrates the IR absorption spectra over the range 400–4000 cm^{-1}, which were measured under vacuum for (a) series A films and (b) series B films, with different T_d. In these spectra, the film thickness values for series A films and those for series B films were almost the same. These spectra were measured within 2 days after deposition. As seen in Figure 4.5a, the absorption bands for both series A and B films were observed at around 650, 800–900, and 2000–2100 cm^{-1}, which are assigned to the wagging, bending, and stretching motions of Si–H bonds, respectively. In addition, for series B films, the stretching motion due to Si–F bonds can be found at around 930 cm^{-1}. The absorption band around 2100 cm^{-1}, observed for series A films, is known to arise from dihydrides (Si–H_2) (Tsu et al. 1989). On the other hand, series B films exhibit an absorption line at around 2100 cm^{-1} having a shoulder at 2000 cm^{-1} that may be due to isolated monohydride (Si–H) (Tsu et al. 1989). The Si–H_2 bonds should exist in the grain boundary regions. Based on these results, the grain boundary in series B films may be more heavily damaged, including a large number of Si–H_2 and Si–H bonds, compared with that in series A films. This result is consistent with the wider Raman spectra for series B films than those for series A films, as seen in Figure 4.4.

Downloaded By: 10.2.97.136 At: 19:24 08 Dec 2023; For: 9781315153544, chapter4, 10.4324/9781315153544-5

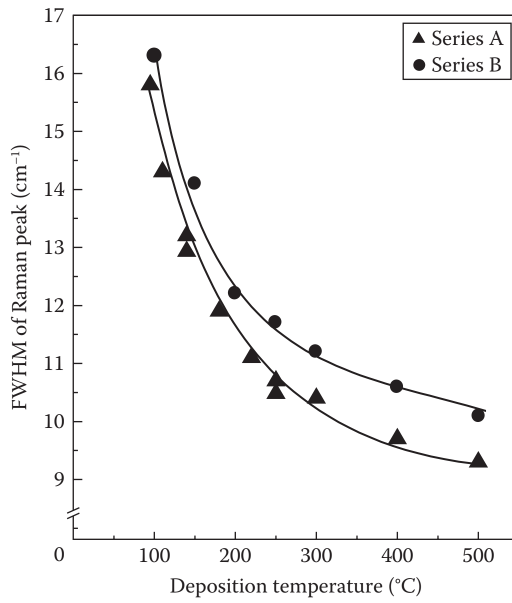

Figure 4.4 Full width at half maximum (FWHM) values, which were obtained from the 520 cm^{-1} Raman signal arising from the crystalline Si phases, as a function of *T*d, for series A films (closed triangles) and series B films (closed circles).

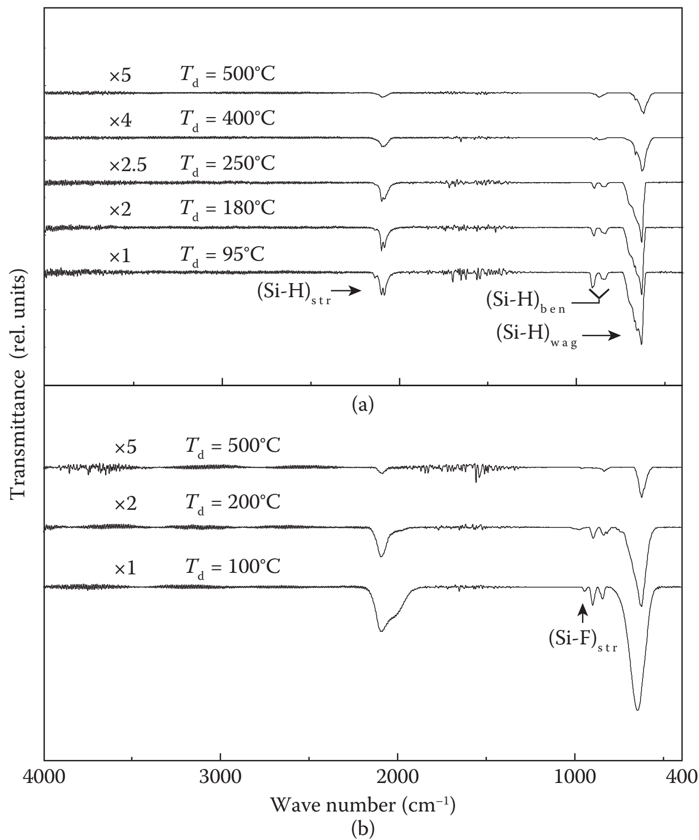

Figure 4.5 IR absorption spectra over the range 400–4000 cm^{-1}, which were measured under vacuum for (a) series A films and (b) series B films, with different *T*d values.

Downloaded By: 10.2.97.136 At: 19:24 08 Dec 2023; For: 9781315153544, chapter4, 10.4324/9781315153544-5

4.4.2 ADDITIONAL DISCUSSION OF THE GROWTH MECHANISMS OF NC-SI

As revealed in Figures 4.1 and 4.2, for the (110) texture, the change in δ with T_d for series A and B films is the same direction with that in the XRD intensity. However, the δ values and the XRD intensity with T_d for the (111) texture of both series films are found to change in the opposite direction. Thus, the (111) nucleation is suggested to be enhanced as the growth of the (111) nuclei is suppressed (Ali et al. 2002). Furthermore, the $\langle\delta(110)\rangle$ values for series B films without H_2 addition are always larger than those for series A films, while the (110) XRD intensities for series B films are smaller than those for series A films. When we examine the results shown in Figures 4.1 through 4.3 in Section 4.1, along with the results shown in Section 4.3 (Toyoshima et al. 1989; Kim et al. 1995; Hasegawa et al. 1998b; Ali et al. 1999; Syed et al. 1999), it is suggested that the $\langle\delta(110)\rangle$ values increase with decreasing H_2 under high T_d (Figure 4.1 and Kim et al. 1995; Milovzorov et al. 1998), but the increase in H_2 under low T_d acts to increase both the (111) and (110) XRD intensities and ρ (Figures 4.2 and 4.3, and Toyoshima et al. 1989).

On the other hand, the (110) XRD intensities are found to increase with increasing T_d (Figure 4.2 and Toyoshima et al. 1989; Syed et al. 1999). In addition, an increase in SiF_4, under high SiH_4 (or low H_2) conditions and high T_d conditions, is likely to result in an increases in the $\langle\delta(110)\rangle$ values and the (110) XRD intensities (Figure 4.1 and Syed et al. 1997), but in a decrease in the $\langle\delta(111)\rangle$ values (Figure 4.1a). However, under low T_d a dominant (111) texture is likely to occur (Figure 4.2 and Hasegawa et al. 1998b; Milovzorov et al. 1998; Ali et al. 1999), though the strength depends on the deposition conditions, such as H_2 (Milovzorov et al. 1998), SiF_4 (Ali et al. 1999), and T_d (Hasegawa et al. 1998b). Supposing that the change in the dominant textures is due to a chemical etching effect (Section 4.3; mechanism 1 or 3), the dominant (110) texture with increasing T_d, corresponding to the conditions for obtaining the results shown in Figure 4.2 and Syed et al. (1997), may be caused by the enhancement in the etching due to the SiF_4 addition to the feed gases (Lim et al. 1996). However, the dominant (111) texture is due to the conditions of low T_d.

Based on these results, the occurrence and the growth of <110>-textured grains and the $\langle\delta(111)\rangle$ values appear to be enhanced and reduced, respectively, as T_d increases under low H_2 and high SiF_4 conditions. On the other hand, the occurrence and the growth of (111) grains appear to be enhanced as T_d decreases under high H_2 and low SiF_4 conditions. Furthermore, a large number of H atoms were incorporated in films with high SiF_4 values under low T_d conditions. However, as H_2 gas is added to the feed gases along with SiF_4, similar to those for series A films, the effect of the F-radicals will be eliminated as stated in Section 4.3. Such a difference in the crystalline properties due to the SiF_4 or H_2 addition under different T_d conditions may be caused by a difference in the etching rate depending on T_d, that is, under low T_d conditions the etching due to H-radicals is enhanced (Kim et al. 1991), and under high T_d the etching due to F-radicals is enhanced (Lim et al. 1996). Since F-radicals are more reactive than H-radicals, F-radical may cause more roughened surface than H-radicals. This model (mechanism 3 in Section 4.3) may be why the role of H-radicals is different from that of F-radicals, depending on T_d. However, the roles of H- and F-radicals in plasma on the crystalline properties appear to be different from each other. So, in order to make clear the roles of H- and F-radicals in plasma, more detailed examinations for films with different H_2 or SiF_4 values will be required.

As shown in Figure 4.3a, the Raman spectra for both series films exhibit similar T_d dependence, and E_R for series A films are found to approach $E_R = 522\ cm^{-1}$ at $T_d = 300°C$, whose E_R value is close to that found for single c-Si. However, the maximum E_R value for series B films is $526\ cm^{-1}$ at $T_d = 300°C$. If the Raman shifts are controlled by a fluctuation of the electronic polarization for constituents in the films, depending on the bonding structure such as atomic distance, the Raman peak shifts would be related to a change in the stress of the films: an increase in the compressive stress or a decrease in the tensile stress should result in a positive Raman shift. Furthermore, if the Raman shift is due only to the confinement of optical phonons in spherical small grains, the peak shift can be expressed as a function of the effective grain size, D_R (Edelberg et al. 1997). Thus, the changes of E_R may reflect a change in stress or in δ. Then, the change in E_R smaller than $522\ cm^{-1}$ found for series A films may be interpreted in terms of different δ values (Edelberg et al. 1997). However, the values of $E_R = 526\ cm^{-1}$ found for series B films may be interpreted in terms of a change in the stress rather than that due to different δ value. The result found for

Downloaded By: 10.2.97.136 At: 19:24 08 Dec 2023; For: 9781315153544, chapter4, 10.4324/9781315153544-5

the series B films may be related to the high etching rate by F-radicals under high T_d (Lim et al. 1996), causing mechanism 3 in Section 4.3. This effect will also result in occurrence of the dominant (110) texture as stated above.

By contrast, as seen in Figure 4.4, the FWHM of the Raman spectrum for both series films monotonically decrease with increasing T_d. Based on the mechanisms causing the Raman shift, the FWHM values will, in general, broaden as random stress exists in a film or as grains with different δ values are widely distributed. As stated above, the Raman shift for series A films may be mainly caused by different δ, and the shift under high T_d conditions for series B films may be due to the different stress. In addition, the FWHM values for series B films in a high T_d range are found to be significantly larger than those for series A films, as shown in Figure 4.4. Therefore, the excess roughening of the substrate surface (mechanism 3 in Section 4.3) due to F-radicals for series B films may also cause the increase in the random stress, in addition to the effect of the change in stress causing a large positive Raman shift under high T_d conditions (Figure 4.3a), as stated above.

4.5 CONCLUSION

We deposited nc-Si films by a PECVD method using SiF_4/SiH_4 /H_2 gas mixtures. The structural properties of the nc-Si films were examined by increasing T_d from ~100 to 500°C for two different series with H_2 = 30 sccm and SiF_4 = 0.38 sccm as series A films, and with H_2 = 0 sccm and SiF_4 = 0.5 sccm as series B films. The interesting feature in the present work lies in making clear the crystallization process, through the understanding of the roles of H- and F-radicals in plasma under different T_d conditions. So, the structural properties were examined for PECVD nc-Si films with different H_2, SiF_4, and T_d values, comparing with those in the previously published works. As described in Sections 4.3 and 4.4.2, occurrence of the different textures may have a close relationship with a change in the structural properties, such as the shifts of the Raman spectra due to the c-Si phase, the changes in the FWHM, and the different stress and bonding properties.

The occurrence and the growth of (110)-textured grains and the <δ(111)> values appear to be enhanced and reduced, respectively, as T_d increases under low H_2 and high SiF_4 conditions. On the other hand, the occurrence and the growth of (111)-textured grains are enhanced as T_d decreases under high H_2 and low SiF_4 conditions. Such a difference in the crystalline properties due to the SiF_4 or H_2 addition under different T_d conditions may be caused by a difference in the etching rate depending on T_d. The changes in other structural properties, such as the above-stated physical parameters, with varying H_2 and SiF_4 values under different T_d conditions were also examined, and the results were interpreted in terms of the model for interpreting the changes in the texture as stated above. This model would be closely related to mechanism 3 shown in Section 4.3.

REFERENCES

Ali AM, Inokuma T, Kurata Y, Hasegawa S. (1999). Effects of addition of SiF_4 during growth of nanocrystalline silicon films deposited at 100°C by plasma-enhanced chemical vapor deposition. *Jpn. J. Appl. Phys.* 38: 6047–6053.

Ali AM, Inokuma T, Kurata Y, Hasegawa S. (2001). Luminescence properties of nanocrystalline silicon films. *Mate. Sci. Eng. C.* 15: 125–128.

Ali AM, Inokuma T, Kurata Y, Hasegawa S. (2002). Structural and optical properties of nanocrystalline silicon films deposited by plasma-enhanced chemical vapor deposition. *Jpn. J. Appl. Phys.* 41: 169–175.

Arai T, Nakamura T, Shirai H. (1996). Initial stage of microcrystalline silicon growth by plasma-enhanced chemical vapor deposition. *Jpn. J. Appl. Phys.* 35: L1161–L1164.

Baert K, Deschepper P, Poortmans J, Nijs J, Mertens R. (1992). Selective Si epitaxial growth by plasma-enhanced chemical vapor deposition at very low temperature. *Appl. Phys. Lett.* 60: 442–444.

Cullity BD. (1978). *Elements of X-Ray Difffraction*, 2nd edn., Addison-Wesley, Reading, p. 102.

Edelberg E, Bergh S, Naone R, Hall M, Aydil ES. (1997). Luminescence from plasma deposited silicon films. *J. Appl. Phys.* 81: 2410–2417.

Hasegawa S, Sakata M, Inokuma T, Kurata Y. (1998b). Effects of deposition temperature on polycrystalline silicon films using plasma-enhanced chemical vapor deposition. *J. Appl. Phys.* 84: 584–588.

Hasegawa S, Uchida N, Takenaka S, Inokuma T, Kurata Y. (1998a). Initial growth of polycrystalline silicon films on substrates subjected to different plasma treatments. *Jpn. J. Appl. Phys.* 37: 4711–4717.

Downloaded By: 10.2.97.136 At: 19:24 08 Dec 2023; For: 9781315153544, chapter4, 10.4324/9781315153544-5

Hasegawa S, Yamamoto S, Kurata Y. (1990). Control of preferential orientation in polycrystalline silicon films prepared by plasma-enhanced chemical vapor deposition. *J. Electrochem. Soc.* 137: 3666–3674.
Hu YZ, Zhao CY, Basa C, Gao WX, Irene EA. (1996). Effects of hydrogen surface pretreatment of silicon dioxide on the nucleation and surface roughness of polycrystalline silicon films prepared by rapid thermal chemical vapor deposition. *Appl. Phys. Lett.* 69: 485–487.
Kakinuma H, Mohri M, Tsuruoka T. (1995). Mechanism of low-temperature polycrystalline silicon growth from a $SiF_4/SiH_4/H_2$ plasma. *J. Appl. Phys.* 77: 646–652.
Kim SC, Jung MH, Jang J. (1991). Growth of microcrystal silicon by remote plasma chemical vapor deposition. *Appl. Phys. Lett.* 58: 281–283.
Kim SK, Park KC, Jang J. (1995). Effect of H_2 dilution on the growth of low temperature as-deposited poly-Si films using $SiF_4/SiH_4/H_2$ plasma. *J. Appl. Phys.* 77: 5115–5118.
Kondo M, Toyoshima Y, Matsuda A. (1996). Substrate dependence of initial growth of microcrystalline silicon in plasma-enhanced chemical vapor deposition. *J. Appl. Phys.* 80: 6061–6063.
Lee KE, Lee WH, Shin SC, Lee C. (1996). Microcrystalline silicon films deposited by electron cyclotron resonance plasma chemical vapor deposition using helium gas. *Jpn. J. Appl. Phys.* 35: L1241–L1244.
Lim HJ, Ryu BY, Ryu JI, Jang J. (1996). Structural and electrical properties of low temperature polycrystalline silicon deposited using SiF_4-SiH_4-H_2. *Thin Solid Films* 289: 227–233.
Matsuda A. (1983). Formation kinetics and control of microcrystallite in μc-Si:H from glow discharge plasma. *J. Non-Cryst. Solids* 59&60: 767–774.
Meyerson BS, Himpsel F, Uram K. (1990). Bistable conditions for low-temperature silicon epitaxy. *Appl. Phys. Lett.* 57: 1034–1036.
Milovzorov D, Inokuma T, Kurata Y, Hasegawa S. (1998). Relationship between structural and optical properties in polycrystalline silicon films prepared at Low temperature by plasma-enhanced chemical vapor deposition. *J. Electrochem. Soc.* 145: 3615–3620.
Nagahara T, Fujimoto K, Kano N, Kashiwagi Y, Kakinori H. (1992). In-situ chemically cleaning poly-Si growth at low temperature. *Jpn. J. Appl. Phys.* 31: 4555–4558.
Nagamine K, Yamada A, Konagai M, Takahashi K. (1987). Epitaxial growth of silicon by plasma chemical vapor deposition at a very low temperature of 250°C. *Jpn. J. Appl. Phys.* 26: L951–L953.
Okada Y, Chen J, Campbell IH, Fauchet PM, Wagbner S. (1989). Mechanism of microcrystalline silicon growth from silicon tetrafluoride and hydrogen. *J. Non-Cryst. Solids* 114: 816–818.
Srinivasan E, Parsons GN. (1998). Hydrogen abstraction kinetics and crystallization in low temperature plasma deposition of silicon. *Appl. Phys. Lett.* 72: 456–458.
Syed M, Inokuma T, Kurata Y, Hasegawa S. (1997). Effects of the addition of SiF_4 to the SiH_4 feed gas for depositing polycrystalline silicon films at low temperature. *Jpn. J. Appl. Phys.* 36: 6625–6632.
Syed M, Inokuma T, Kurata Y, Hasegawa S. (1999). Temperature effects on the structure of polycrystalline silicon films by glow-discharge decomposition using SiH_4/SiF_4. *Jpn. J. Appl. Phys.* 38: 1303–1309.
Toyoshima Y, Arai K, Matsuda A. (1989). Lattice orientation of microcrystallites in μc-Si:H. *J. Non-Cryst. Solids* 114: 819–821.
Tsai CC, Anderson GB, Thompson R, Wacker B. (1989). Control of silicon network structure in plasma deposition. *J. Non-Cryst. Solids* 114: 151–153.
Tsu DV, Lucovsky G, Davidson BN. (1989). Effects of the nearest neighbors and the alloy matrix on SiH stretching vibrations in the amorphous SiOr:H ($0<r<2$) alloy system. *Phys. Rev. B* 40: 1795–1805.
Tsu R, Gonzalez-Hernandez J, Chao SS, Lee SC, Tanaka K. (1982). Critical volume fraction of crystallinity for conductivity percolation in phosphorus-doped Si: F: H alloys. *Appl. Phys. Lett.* 40: 534–535.

Downloaded By: 10.2.97.136 At: 19:24 08 Dec 2023; For: 9781315153544, chapter4, 10.4324/9781315153544-5